Sett et al. *Microsystems & Nanoengineering* (2026)12:309
https://doi.org/10.1038/s41378-026-01396-w

Microsystems & Nanoengineering
www.nature.com/micronano

ARTICLE Open Access

# Single bi-functional flexible sensor device for simultaneous pH and oxygen monitoring during pre-transplant normothermic perfusion

Avik Sett[1,2], Filippos Bersis[1], Puck Groen[3], Annelot Muntinga[3], Jeroen de Jonge[3], Robbert Friendwijk[1], Ger de Graaf[1], Massimo Mastrangeli[1] and Paddy French[1]✉

**Abstract**

Monitoring of organ health and tissue damage through real-time sensing of chemical parameters such as pH and oxygen concentration could provide helpful information in the field of solid organ transplantation. Several sensors have been developed to detect oxygen concentrations and pH levels in tissues separately; however, there is no report to date on a single device in such context that can detect both pH and oxygen alterations simultaneously and in real time. This paper reports the development of a single, bi-functional optical sensor device that can simultaneously and reversibly respond to changes in both pH and oxygen concentration. The proposed optical sensor integrates both pH- and oxygen-sensitive probes, and is optimized to achieve minimal cross-sensitivity during simultaneous measurements. The sensor is excited with light of 405 nm wavelength to detect pH and oxygen changes respectively at emission wavelengths of 520 nm and 600 nm. The sensor detects pH and oxygen alterations with a response time of about 12.5 s and less than 1.5 s, respectively. The sensor exhibits a sensitivity of 75.75% for pH variations and 20.4% per mg/ml for changes in oxygen concentration. The sensor was tested on a human liver declined for transplantation to analyse the initial sensor behaviour on human tissue. Including the sensor in an organ perfusion setup to monitor pH and oxygen levels could potentially provide insight into the microcirculation of an organ before transplantation.

## Introduction

In the field of solid organ transplantation, dynamic preservation by machine perfusion has emerged as a promising technique to enhance organ preservation and enable functional assessment prior to transplantation. Although ex situ perfusion strategies vary widely between organs, with differences in timing, perfusate composition, perfusate temperature and perfusion duration, monitoring of key physiological parameters such as pH and partial pressure of oxygen in the perfusate is widely implemented[1,2]. These measurements in the perfusate offer insight into what is provided to the organ and are used as surrogate markers for tissue-level physiology. However, it remains unclear how these measurements reflect the physiological state of the organ at a peripheral and tissue level. Monitoring of closely related metabolic biomarkers at the same tissue site, may improve assessment of organ viability. Simultaneous measurement of oxygen and pH at a central and peripheral level can provide insight into the differences in central circulation and microcirculation of an organ. This demands a compact and miniaturized sensor system with minimal wiring to avoid microbial contamination in a closed perfusion system.

State-of-the-art oxygen sensors, like the Clark oxygen electrode, reduce oxygen on a noble metal electrode[3]. Even though the sensors exhibit good accuracy, they suffer from long-term drift and high cost. Moreover, these systems consume oxygen during measurement, resulting in erroneous data readout in case of low-level oxygen detection. An alternative approach to detect oxygen levels

Correspondence: Paddy French (p.j.french@tudelft.nl)
[1]Department of Microelectronics, Delft University of Technology, Mekelweg 4, 2628 CD Delft, The Netherlands
[2]School of Electrical and Computer Sciences, Indian Institute of Technology (IIT), Bhubaneswar, India
Full list of author information is available at the end of the article

employs the principle of fluorescence quenching[4]. The quenching follows the Stern-Volmer equation as given in Eq. (1):

$$I/I_0 = 1 + K_{sv}[Q] \quad (1)$$

where $I_0$ and I are fluorescence intensities in absence and presence of oxygen, respectively, the concentration of oxygen is denoted as Q, and $K_{sv}$ represents the Stern-Volmer constant.

Among fluorophores, ruthenium-based transition metal complexes are commonly used in oxygen detection due to their high quantum yield, large dynamic range, low level detection and high photostability. These complexes are suspended into a variety of matrices for fabrication of oxygen sensors. Silica gels[5], silicone rubbers[6–9], polymers[10–13] and sol-gels[14–20] are common matrices to bind the ruthenium complex. Kumar et al. embedded ruthenium compound on a Pluronic F127 matrix and monitored intracellular and intratumoral oxygen gradients[21]. McEvoy et al. fabricated a dissolved oxygen sensor by incorporating oxygen sensitive ruthenium complexes in a sol-gel derived porous silica coating[22], but largely fails to address the comprehensive organ monitoring that requires the simultaneous tracking of multiple biomarkers (e.g., $O_2$, pH, $CO_2$) across various regions of the graft. Lin et al. proposed a hydrogel based stretchable oxygen sensor for wearable applications. The sensor exhibited strain insensitive oxygen detection with very high sensitivity[23]. Kermis et al. developed a robust pH sensor[24] using methacryloyl modified 8-hydroxy-1,3,6-pyrene trisulfonic acid (HPTS). Sensors were prepared by copolymerization of the MA-HPTS with poly(ethylene glycol) diacrylate. The sensor exhibited good optical response towards pH in the range between 6-9. However, relying on discrete, single-parameter sensors crowds the organ surface, multiplies the external optical hardware required in the operating room, and inherently drives up overall system costs. De-Graaf et al. fabricated pH sensor based on HPTS loaded microbeads in hydrogel to detect myocardial ischemia during open heart surgery[25], however the sensor had severe drift issues with time. Few ratio-metric approaches aimed at minimizing cross-sensitivity have been proposed earlier[21], however, placing a pH sensor on one section of the tissue and an oxygen sensor on another, fails to capture the interdependent relationship between these biomarkers. It yields geographically disjointed data rather than a true representation of localised cellular health. Previous reports mostly focused on the fabrication of dedicated pH and oxygen sensors based on fluorescent probes similar to those adopted here, namely ruthenium and pyranine[22–25]. While discrete optical sensors for oxygen and pH are well-documented, the synthesis of a single, chemical-based, and entirely biodegradable hydrogel matrix capable of capturing both biomarkers simultaneously has not been previously achieved. A multifunctional sensor acquires different metabolic parameters at the same location simultaneously. This co-localisation provides a synchronised, high-fidelity metabolic snapshot of that specific tissue microenvironment, allowing for a much more accurate assessment of graft viability. This research focuses on integration of both sensing probes (ruthenium and HPTS) into a single hydrogel matrix to achieve simultaneous detection of oxygen and pH changes. This integration represents a significant technological leap, enabling the continuous, co-localised extraction of critical metabolic data using a single, biocompatible footprint.

In this work, the ruthenium complex was immobilized into a hydrogel matrix, which is proven to be biocompatible and does not require activation. 8-Hydroxypyrene-1,3,6-trisulphonic acid trisodium salt (HPTS), also called pyranine, was selected as pH-sensitive probe due to high pH sensitivity, large Stokes shift and proven compatibility with hydrogels[25]. Integrating pH and $O_2$ sensors on a single substrate enables local, simultaneous monitoring of two closely related metabolic biomarkers at the same tissue site, improving assessment of organ viability. While the overall setup is not space-limited, the normothermic machine perfusion system has constrained space around the organ, making compact sensor design and reduced wiring important. This also facilitates the future use of multiple sensor units distributed across the organ. Furthermore, clinical perfusion protocols require a closed, sterile chamber, and sensor integration minimizes wiring and feedthroughs, improving sterility and clinical applicability. In addition, miniaturization of the size of the device and its compactness, allows for its extended use on smaller transplantable organs such as kidneys.

Ruthenium and pyranine are usually utilized as fluorescent probes through encapsulation in polymers[23–25]. Oxygen-sensitive ruthenium incurs fluorescence quenching in presence of oxygen, whereas the pH probes undergo higher absorption at higher pH levels, leading to enhanced fluorescence intensity. A rapid drop in oxygen levels lead to ischemia and subsequent tissue damage. Hypoxia forces cells to switch from aerobic to anaerobic metabolism, resulting in the accumulation of lactic acid and a decrease in intracellular pH[26–29]. Consequently, the ratio of oxygen-dependent fluorescence intensity (at 600 nm wavelength) to pH-dependent fluorescence intensity (at 520 nm) increases. Under normoxic conditions, oxygen delivery and consumption are balanced and pH is physiological, resulting in a low oxygen-to-pH ratio. Ratio-metric analysis of the fluorescence intensity can help monitoring the microcirculatory perfusion and detecting hypoxia within tissues. The overall schematic of

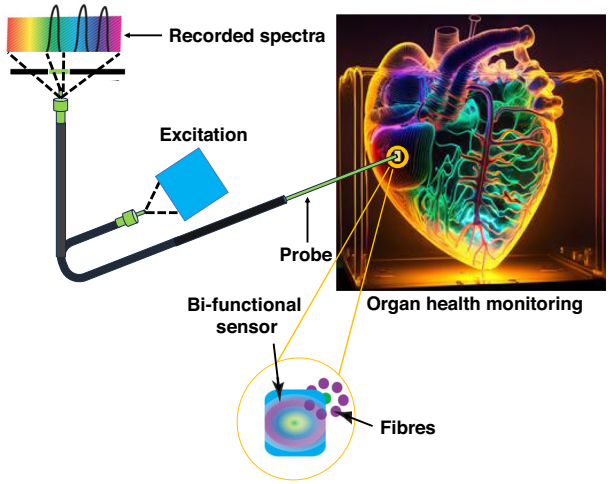


**Fig. 1** Schematic of the overall sensing principle for organ health monitoring

the complete sensing mechanism is represented in Fig. 1. The excitation source excites the optical probes in the sensor layer, which behaves differently for different physiological conditions. The variable behaviour of the sensor is captured as intensity variation of the collected spectrum. Table 1 compares the performance of the fabricated sensor with some existing sensors in literature.

## Sensor fabrication and experimental methods

### Choice of sensor matrix and sensor probes

A polyurethane-based hydrogel (HydroMed D4 from AdvanSource Biomaterials) was selected as the sensor matrix to encapsulate the sensor probes. The proven biocompatibility and non-essential activation process for HydroMed D4 was significant in choosing the sensor matrix. The HydroMed D4 is dissolved in ethanol for its development. The sensor probes, i.e. fluorescent particles/complex, are introduced into the hydrogel solution to form an integrated system of sensing elements encapsulated in a sensor matrix. The hydrogel layers encapsulating the sensor probes have a lifetime of more than 40 days[30]. These attributes make HydroMed D4 a promising candidate in sensor applications[31].

Pyranine (HPTS) is a phenolic luminophore which contains phenol or phenolates as its functional attachment. Photoexcitation of phenolate groups results in fluorescence. A decrease in pH contributes to smaller absorption of the phenolate form leading to reduction in fluorescence. On the contrary, an increase in pH results in enhancement of fluorescence. Pyranine was selected due to its high sensitivity towards pH alterations, large Stokes shift and ease in processing. However, pyranine suffers from bleaching and alters the ionic strength of the solution. Hence, proper encapsulation of the pyranine in the sensor matrix is of utmost importance.

Ruthenium complex is chosen as fluorescent probes for oxygen detection owing to their high sensitivity towards oxygen, large Stokes shift and excellent selectivity. In the absence of oxygen, the ruthenium complex exhibit very high fluorescence intensity after excitation. However, in presence of oxygen, the excited states of the ruthenium complex collide with the triplet state of oxygen molecules, resulting in fluorescence quenching[24]. The ruthenium complex is embedded within the hydrogel matrix to avoid any possibility of toxicity local to the hydrogel. The decrease in fluorescence intensity with increase in oxygen concentration gives an indication of the oxygen levels in a given media.

### Fabrication of sensors

For successful fabrication of the sensors, a lubricious hydrophilic polyurethane, HydroMed D4 was procured from AdvanSource Biomaterials, 8-Hydroxypyrene-1,3,6-trisulfonic acid (HPTS) and Dichlorotris (1,10-phenanthroline) ruthenium (II) hydrate was procured from Merck Sigma. AmberChrom microbeads for HPTS functionalization was supplied by DuPoint.

#### *Fabrication of pH-sensing layers*

The fabrication of the pH sensor is shown in Fig. 2. Initially 10 g of AmberChrom microbeads (from DuPont) were soaked in 10 ml demineralized (DM) water. 35 mg HPTS (pyranine) was dissolved in 100 ml DM water and the microbead solution was added to it. The resulting solution was stirred for 15 h at 400 rpm. During this process, HPTS got functionalized on the microbeads surface. The microbeads with HPTS were collected through filtration. The hydrogel matrix was prepared by dissolving 1 g HydroMed D4 precursor into 10 ml 90% ethanol. The solution was stirred for about 6 h to get a uniform hydrogel solution. 3.5 g of the HPTS-functionalized microbeads was added to 10 ml of hydrogel solution. The mixture was stirred for 6 h to get a well-dispersed profile of microbeads in the hydrogel. The solution was then drop-casted over a glass slide, followed by drying at room temperature to prepare the pH-sensing layer.

#### *Fabrication of oxygen-sensing layers*

Dichlorotris (1,10-phenanthroline) ruthenium (II) hydrate was selected as the precursor for fabrication of the oxygen sensor, shown in Fig. 3. 50 mg of the ruthenium complex was dissolved in 10 ml solution of methanol and toluene (4:1). The solution was stirred for 1 h at 100 rpm. 1 ml of the as-prepared ruthenium solution was added to 10 ml of hydrogel solution. The resulting mixture was stirred for 1 h at 300 rpm to obtain a uniform mixture of ruthenium complex in hydrogel solution. The solution

**Table 1 Comparison of existing sensor performances**

| Sensor Name | Sensor Technology | Spatial Footprint | Sensitivity | Cross-Sensitivity/Interferences | Response Time | Application Context |
|---|---|---|---|---|---|---|
| Luminescence pH Optrode[33] | Optical (Luminescence) | Macroscopic (1-cm pathlength cuvette). | pH 1-8 dynamic range; ±0.1 pH unit accuracy. | Black filter prevents light scattering and background interference from opaque media/cells. | n/a | Anaerobic fermentation monitoring. |
| Biodegradable Microsensor[32] | Electrochemical (Galvanic couple) | 15 ×18 mm (0.45 $cm^2$ active area). | ~6 mV / % O2 (0-60 atm% range). | Anode passivation requires high-current cleaning; sensitive to background electrolytes. | Steady-state (requires 2-min recovery step). | Transient in vivo and environmental sensing. |
| Fiber-optic $O_2$ Sensor[34] | Optical (Fluorescence quenching) | Micrometer-scale (3–100 µm fiber cores). | 0-15 ppm O2; LOD ~ 0.3 ppm. | Covalent bonding stops dye leaching; electronic shutter reduces photobleaching. | ~1 s | In-situ environmental and biomedical $O_2$. |
| Glass Metabolic Chip (GC3)[35] | Electrochemical (Amperometric O2, Potentiometric pH) | O2: 25 µm diameter; pH: 1.24 ×0.46 mm. | O2: -0.08 to -2.35 nA; pH: ~45 mV / pH step. | Reduced voltage avoids redox interference; pH sensor exhibits baseline drift. | O2: 5 s; pH: <20 s | In vitro cell metabolism tracking. |
| IMPACT $O_2$ Sensor[36] | Electrochemical (Clark-type) | 2.8 ×5.0 ×1.4 mm overall. | Distinct current shifts at 10%, 21%, and 100% O2. | Nafion coating mitigates biofouling and foreign body response. | 1-2 min | In vivo intestinal $O_2$ (anastomotic leak detection). |
| 3D Hydrogel Waveguide[37] | Optical (Diffractive grating) | Micro/Nanoscale (1-5 µm waveguide width). | High contrast (signal intensity drops to ~0 upon swelling). | Highly cross-sensitive to both ionic strength and humidity/water. | pH: Seconds; Water: ~210 min. | Lab-on-a-chip; environmental humidity. |
| PEG-DA Hydrogel Optical $O_2$[38] | Optical (Fluorescence quenching) | 250 µm thick film on glass. | Linear response ($R^2$ = 0.995) from 0-21% O2. | PEG-DA minimizes biofouling; modulated LED rejects ambient light. | ~1 s | Cell culture bioreactor monitoring. |
| Tissue Spectroscope (TiSpec)[39] | Optical (NADH fluorescence, Laser Doppler, Reflectance) | Macroscopic ( ~ 0.6 mm tissue sphere) | Highly linear correlation ($R^2$ = 0.992) with clinical fluorometers. | Blood volume alters NADH signal; corrected via reflectance subtraction. | ~3 s | In vivo tissue vitality monitoring. |
| **Bifunctional semsor (This work)** | **Optical (Fluorescence)** | **1 cm x1cm** | **75.75% for pH and 20.4% for oxygen** | **None** | **12.5 s for pH and 1.5 s for oxygen** | **pre-transplant normothermic perfusion** |

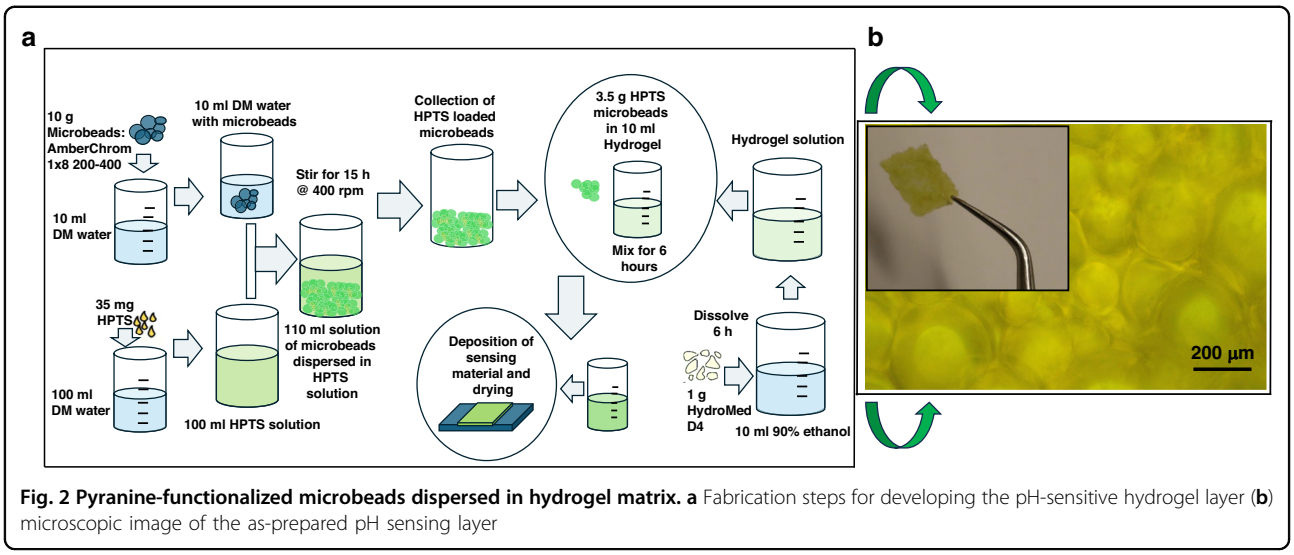


**Fig. 2 Pyranine-functionalized microbeads dispersed in hydrogel matrix. a** Fabrication steps for developing the pH-sensitive hydrogel layer (**b**) microscopic image of the as-prepared pH sensing layer

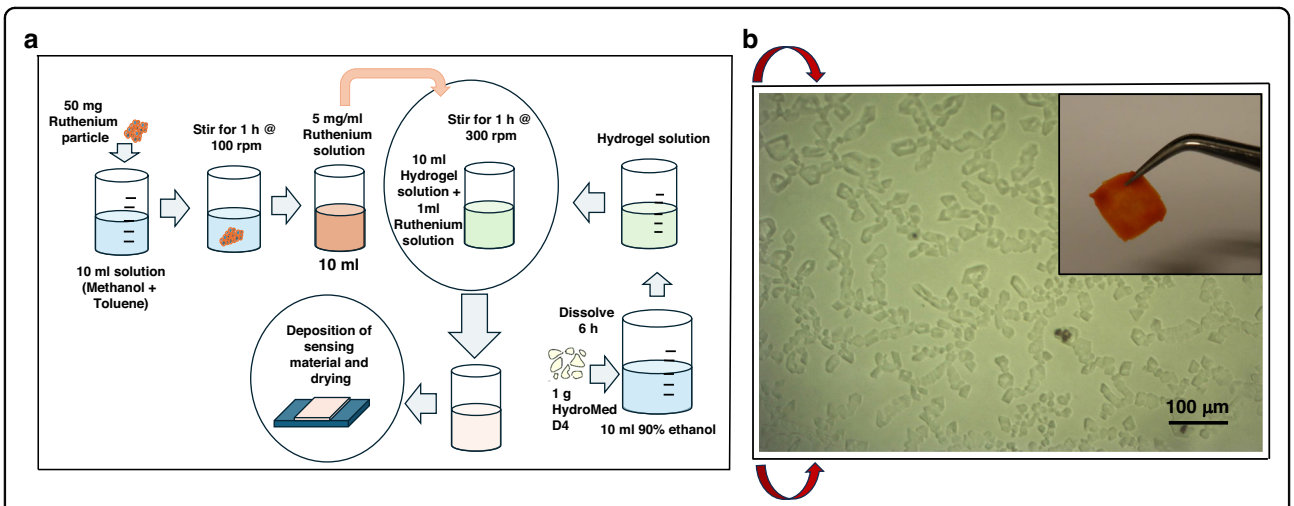


**Fig. 3 Ruthenium complex dispersed in hydrogel matrix. a** Fabrication steps for developing the oxygen-sensitive hydrogel layer (**b**) microscopic image of the as prepared oxygen sensing layer

was then drop casted-over a glass slide and allowed to dry to prepare the oxygen-sensing layer.

### *Fabrication of the bi-functional pH and oxygen sensor*

Fabrication of a single, bi-functional sensor with both pH- and oxygen-sensitive probes was targeted, and is shown in Fig. 4. Initially, 10 g of AmberChrom microbeads were soaked in 10 ml DM water. 35 mg HPTS was dissolved in 100 ml DM water and the microbead solution was added to it. The resulting solution was stirred for 15 h at 400 rpm. The microbeads with HPTS were collected through filtration. 200 mg of the ruthenium complex was dissolved in 5 ml solution of methanol and toluene (4:1). The solution was stirred for 1 h at 100 rpm to obtain "Ru40" solution. The hydrogel matrix was prepared by dissolving 1 g HydroMed D4 precursor into 10 ml 90% ethanol. The solution was stirred for about 6 h to get a uniform hydrogel solution. 3.5 g of the HPTS-functionalized microbeads along with 1 ml of Ru40 were added to 10 ml of hydrogel solution. The mixture was stirred for 6 h to get a well-dispersed profile of ruthenium and microbeads in the hydrogel. The solution was then drop-casted over a glass slide, followed by drying at room temperature to prepare the bi-functional sensing layer. The concentration of ruthenium complex was optimized keeping the HPTS concentration fixed. For other concentrations of ruthenium, *i.e.*, 5 mg/ml, 10 mg/ml, 25 mg/ml and 50 mg/ml, severe cross-sensitivity issues were observed. This means that while measuring the pH of the solution at fixed oxygen levels, the oxygen-sensitive emission peak (600 nm) undergoes intensity variations. Additionally, while measuring the oxygen levels in the

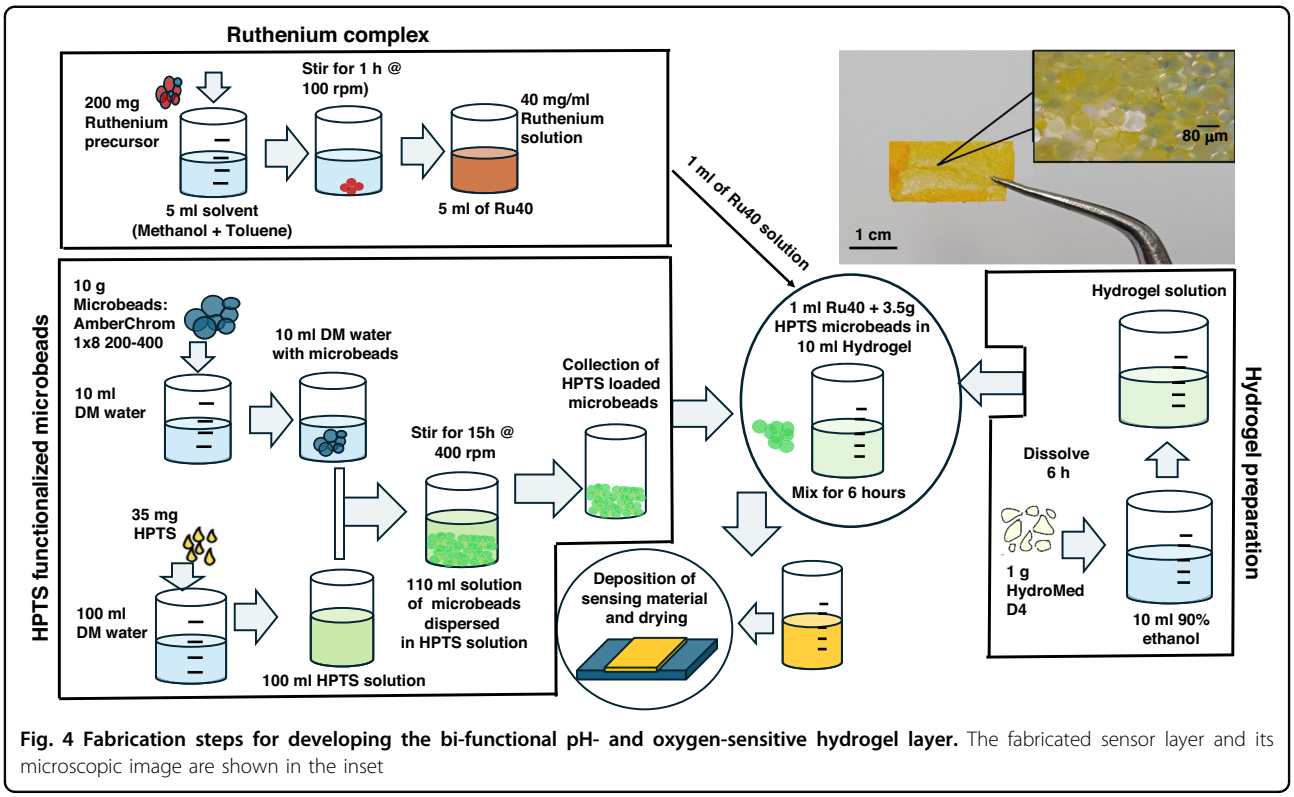


**Fig. 4 Fabrication steps for developing the bi-functional pH- and oxygen-sensitive hydrogel layer.** The fabricated sensor layer and its microscopic image are shown in the inset

solution at a fixed pH value, the pH-sensitive emission peak (520 nm) undergoes severe variations in intensity. The effect of cross-sensitivity is highly minimized at the optimized ruthenium concentration of 40 mg/ml added to the hydrogel precursor. The effective optimized ratio of ruthenium to HPTS in the sensor is 1:88 by weight ($HPTS_{88}Ru$).

## Experimental setup

The experimental setup is sketched in Fig. 5. A controlling circuit for the switching of two light-emitting diodes (LEDs) was implemented on a prototype board of the ESP (Espressif) module (manufactured by Espressif Systems). This module was connected to a computer, and the ESP module and the LEDs were connected to a power supply. The purpose of using two LEDs in the system is to characterize the sensor with 405 and 450 nm illumination and optimize its efficacy for a single sensor system.

As detector, a flame spectrometer was used in combination with an optical fibre. In order to align the LEDs and the spectrometer in such a way that the sensor layer can be illuminated efficiently and the fluorescent emission falls directly on the optical fibre, a double-compartment case was designed in Solid Edge software and later 3D-printed in plastic resin. On one housing part of the case, the LEDs are mounted and a hole is introduced to tightly fit the optical fibre. Onto the other part of the case, working as a cover, the glass slide with the sensor layer is glued. Thereafter, the cover can slide over the housing with the LEDs to compose a closed square case.

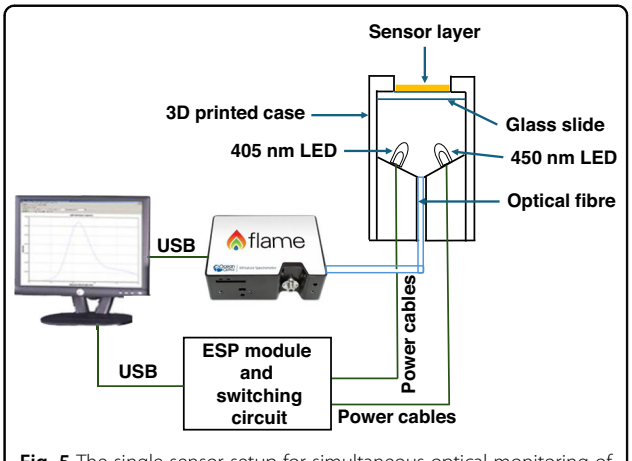


**Fig. 5** The single-sensor setup for simultaneous optical monitoring of both pH and oxygen changes

Figure 6 shows the actual measurement setup used during the experiments. The sensor is connected to the ESP module via power cables to turn the LEDs on and off. The spectrophotometer collects the reflected fluorescence from the sensor for analysis. The sensor is connected to the flame spectrophotometer through an optical fibre to obtain the fluorescent measurements. The spectrophotometer then sends the obtained data to the computer for processing. A MATLAB® script drives the ESP

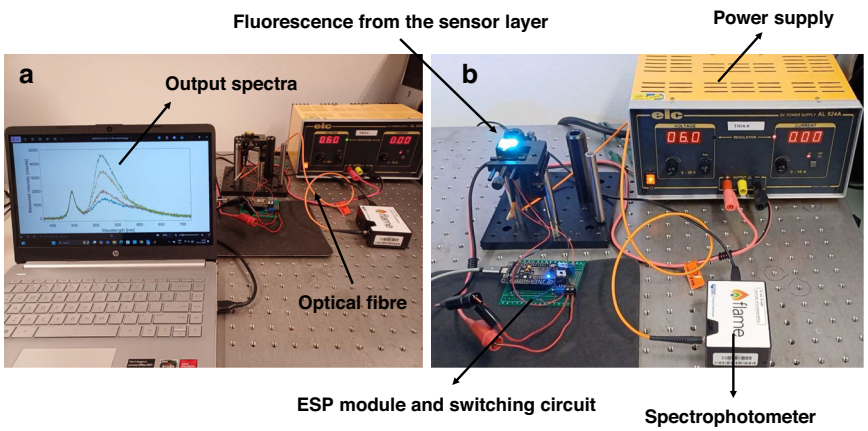


**Fig. 6 Experimental setup. a** The measurement setup comprising power supply, spectrophotometer, microcontroller-based IoT module (ESP32), LEDs and laptop (**b**) zoomed view of the setup with the sensor illuminated with desired wavelength

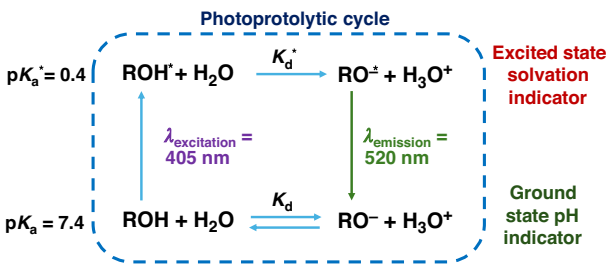


**Fig. 7** Sensing mechanism of pH-sensitive HPTS

module to control the switching of the LEDs during measurements.

### Preliminary measurements on human tissue

To evaluate the sensor behaviour on human tissue, the sensor was tested on an unviable human liver declined for transplantation in the Erasmus Medical Centre, Rotterdam, the Netherlands. The liver was perfused with an acellular perfusion solution, and the supplied oxygen level was manually adapted from 1 L/min to 6 L/min. The preliminary results are discussed in a later section.

## Sensing mechanism

Figure 7 depicts the sensing mechanism of the pH-sensitive HPTS probes. When the HPTS-functionalized microbeads are exposed to solutions with higher pH level, the phenolic groups of HPTS absorb more photons when illuminated with 405 nm light. More molecules undergo excitation and relaxation, leading to higher intensity fluorescence at 520 nm. Thereby, lower pH corresponds to lower fluorescence intensity, and conversely higher pH corresponds to higher fluorescence intensity[25].

The sensing mechanism for the oxygen-sensitive ruthenium complex is elaborated in Fig. 8 and its details can be found in previous articles[8,22]. In brief, the singlet state $S_0$ is the electronic ground state for the ruthenium complex molecule. When light absorption at 405 nm takes place, the molecule is prompted to the first excited singlet state (1), which is short-lived and vibrationally relaxes to the ground state (2) of $S_1$. The molecule may return to the $S_0$ state by non-radiative internal conversion (3). Alternatively, $S_1$ may undergo "spin-forbidden" intersystem crossing (ISC) to the triplet state $T_1$ (4). The molecule then de-excites vibrationally to the ground state of T1 (5) and subsequently relaxes to the singlet state $S_0$ through fluorescence (6) at 600 nm. This mechanism is elucidated in Fig. 8a.

When the ruthenium complex is exposed to molecular oxygen, near-resonant energy transfer takes place between the triplet state T1 of the ruthenium complex and $T_0$ ground state of molecular oxygen (7) as shown in Fig. 8b. The energy transfer leads to excitation of the molecular oxygen from $T_0$ ground state to singlet excited state $S_1$ (8). This leads to fluorescence quenching, as the relaxation mechanism (6) of the molecule is hindered. An increase in oxygen concentration leads to higher collision between molecular oxygen and the triplet state of ruthenium, leading to increased quenching of the fluorescence at 600 nm. Fewer collisions are involved at lower oxygen concentration, leading to a higher fluorescence intensity.

### Sensing results

The sensors were tested in solutions having different pH levels. These solutions were prepared by standard chemical processes. The pH levels were standardized and measured using a pH meter (Atlas Scientific).

At the time of testing, the oxygen level was varied by bubbling nitrogen into the solution. The oxygen level was measured and controlled using a compact Dissolved

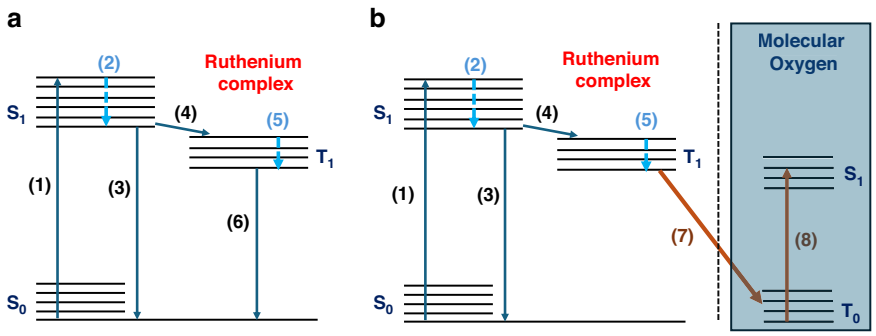


**Fig. 8 Sensing mechanism of oxygen-sensitive ruthenium complex. a** In absence of oxygen (**b**) in presence of oxygen

**Table 2 Optimization of the bi-functional sensor layer**

| Sensing layer | pH sensitivity (per pH) | Oxygen sensitivity (per mg/ml) | Cross-sensitivity towards pH while detecting oxygen | Cross-sensitivity towards oxygen while detecting pH |
|---|---|---|---|---|
| $HPTS_{22}Ru$ | 41.2% | 23.4% | Absent | Present 4% |
| $HPTS_{44}Ru$ | 61.6% | 22.1% | Absent | Present 2.1% |
| **$HPTS_{88}Ru$** | **75.75%** | **20.4%** | **Absent** | **Present 1.23%** |
| $HPTS_{176}Ru$ | 81.8% | 13.6% | Present 25% | Absent |
| $HPTS_{264}Ru$ | 89% | 8% | Present 28.2% | Absent |

The bold row signifies the best sensor combination among others

Oxygen Meter (DO210), manufactured by Extech Instruments.

The fabricated pH and oxygen sensors illustrated in Figs. 2 and 3 were tested initially by illumination with light of both 405 and 450 nm wavelengths. In line with prior literature[19,25], the pH sensor exhibited good sensitivity for pH variations as indicated by the 520 nm emission peak, and the oxygen sensor demonstrated good sensitivity towards oxygen changes at the 600 nm emission peak. The oxygen and pH sensors exhibited better sensitivity when exposed to 405 nm wavelength light compared to 450 nm wavelength. Hence, further experiments were conducted with 405 nm illumination.

The pH levels can range between 6.5 and 8.1 for damaged and healthy tissues, respectively, while the oxygen levels can drop from 2.1 mg/ml to 0 when the tissue encounters severe hypoxia. The aim of this research is to integrate both sensing probes (ruthenium and HPTS) into a single hydrogel matrix to achieve simultaneous detection of oxygen and pH. The content ratio of both sensing probes was adjusted meticulously in order to achieve sufficient sensitivity for both oxygen and pH along with minimal mutual cross-sensitivity. Five such mixing ratios were evaluated, as described in Table 2. The cross-sensitivity for a particular sensor is calculated as follows, where $I_{base}$ is the baseline intensity, ($I_{ox}$ – $I_{base}$) is the unexpected change in intensity for the oxygen peak and ($I_{base}$ – $I_{pH}$) is the unexpected change in intensity for the pH peak during measurement of pH and oxygen, respectively.

Cross sensitivity for oxygen (while measuring pH): ($I_{ox}$ – $I_{base}$) /$I_{base}$ *100; calculated at 600 nm

Cross sensitivity for pH (while measuring oxygen): ($I_{base}$ – $I_{pH}$)/$I_{base}$ *100; calculated at 520 nm

Figure 9a illustrates the cross-sensitivity of the different sensor layers towards pH and oxygen. Minimum cross-sensitivity was observed in the case of $HPTS_{88}Ru$. The pH and oxygen sensitivity of the different sensors are depicted in Fig. 9b.

Figure 10 illustrates the pH and oxygen sensing characteristics for the $HPTS_{176}Ru$ sensing layer. Here, the ratio of ruthenium to HPTS in the sensor is 1:176 by weight ($HPTS_{176}Ru$). Figure 10a elucidates the pH sensing nature of the sensing layer. During pH changes, the amplitude of the 600 nm oxygen-sensitive emission peak remains almost unaltered. The variations in pH can therefore be visualized in the intensity variations of the 520 nm emission peak. With increase in pH levels, both absorption and fluorescence are seen to increase. However, during oxygen level measurement, cross-sensitivity towards pH was observed.

Figure 10b shows that the changes in oxygen level from 5 mg/ml to 8.5 mg/ml incur reduction of fluorescence intensity at the 600 nm peak. Even though the pH of the

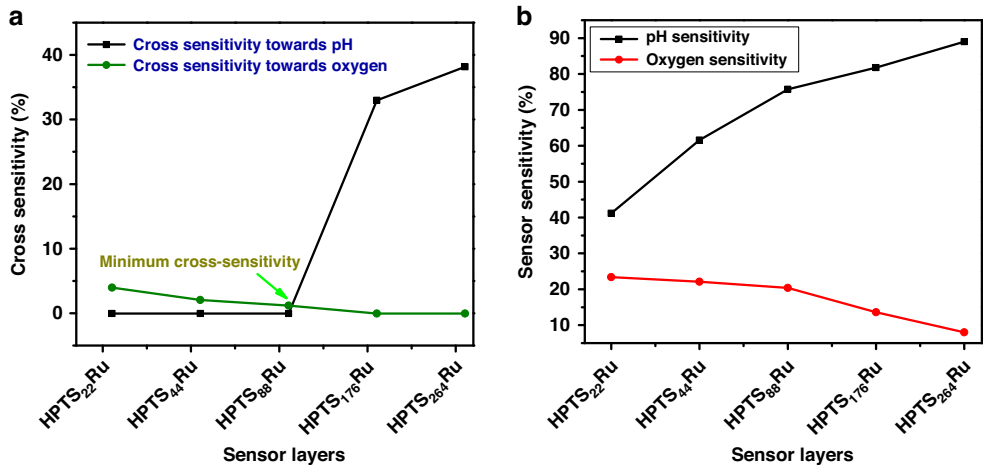


**Fig. 9 Sensitivity of the sensor. a** Cross sensitivity of the sensor layers towards pH and oxygen (**b**) sensor sensitivity towards pH and oxygen

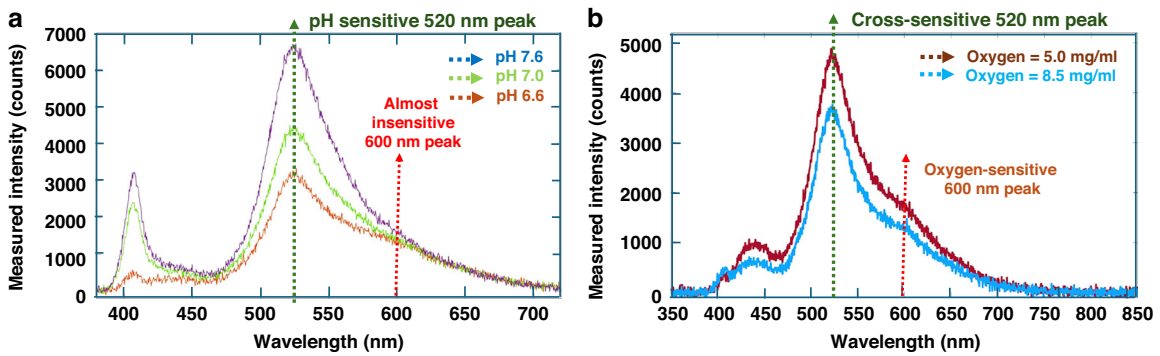


**Fig. 10 Test for cross-sensitivity. a** Detection of pH (at fixed 5 mg/ml oxygen level) by $HPTS_{176}Ru$ with insensitive 600 nm peak. **b** Detection of oxygen levels (at fixed pH value of 7.2) by $HPTS_{176}Ru$ with cross-sensitive 520 nm peak

solution was fixed to 7.2, variation in the 520 nm peak was observed, leading to severe cross-sensitivity. The reduction of intensity at 520 nm peak can be attributed to the smaller amount of ruthenium complex available in the sensor matrix. The presence of oxygen ensures collision with ruthenium along with the phenolic groups of HPTS. However, an increase in ruthenium fraction may ensure that all of the oxygen-related collisions occur with the ruthenium complex only. Hence, further efforts were made to optimize the ratio of the sensor probes such that, during pH measurements, the oxygen peak does not change and, during oxygen measurement, the pH peak does not alter.

Through optimization it was observed that $HPTS_{88}Ru$ shows the best performance in terms of zero cross-sensitivity, pH and oxygen sensitivity. Even though an even higher ratio of ruthenium still supports zero cross-sensitivity, it also causes a fall in pH sensitivity due to lower fraction of HPTS probes. Moreover, the presence of surplus ruthenium does not significantly enhance the oxygen sensitivity. Here, $HPTS_{22}Ru$ and $HPTS_{44}Ru$ suffer low pH sensitivity with only slightly-improved oxygen sensitiveness. Increase in HPTS ratio enhances the pH sensitivity but drastically reduces the oxygen sensitivity and introduces cross-selectivity issues.

Figure 11 demonstrates the pH sensing characteristics of $HPTS_{88}Ru$. This optimized sensing layer exhibits good pH sensitivity at the 520 nm emission peak and shows almost zero sensitivity at the 600 nm one. The pH sensitivity is calculated to be approximately 75.75% per pH, as per Eq. (2). The sensor was tested in the pH range of 6.6 to 8, as this is the common pH physiological range for tissues and organs[32].

$$\text{Sensitivity in pH} = \text{Change in fluorescence intensity}/\text{Baseline intensity} \quad (2)$$

Figure 12 illustrates the oxygen sensing characteristics of $HPTS_{88}Ru$. This optimized sensing layer exhibits excellent oxygen sensitivity at 600 nm and demonstrates

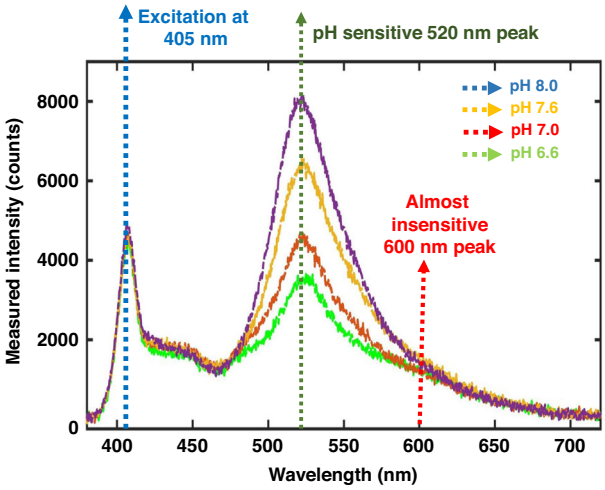


**Fig. 11** Detection of pH (at fixed 5 mg/ml oxygen level) by $HPTS_{88}Ru$ with insensitive 600 nm peak

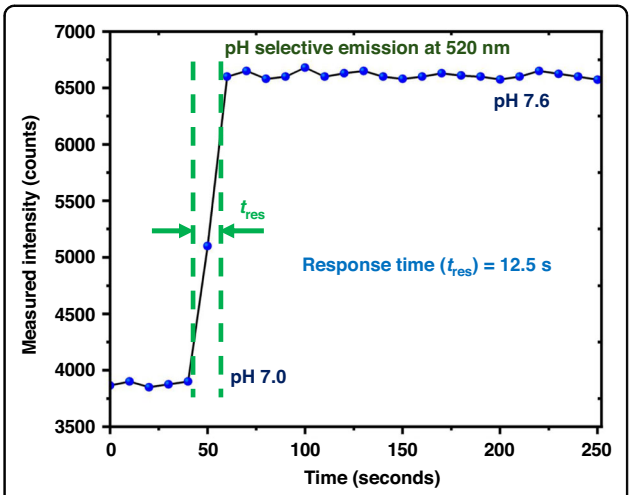


**Fig. 13** Transient response of $HPTS_{88}Ru$ to change in pH from 7.0 to 7.6

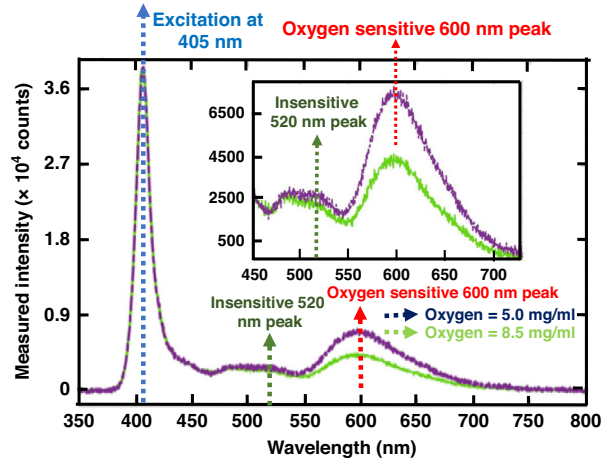


**Fig. 12** Detection of oxygen levels (at fixed pH value of 7.2) by $HPTS_{88}Ru$ with insensitive 520 nm peak

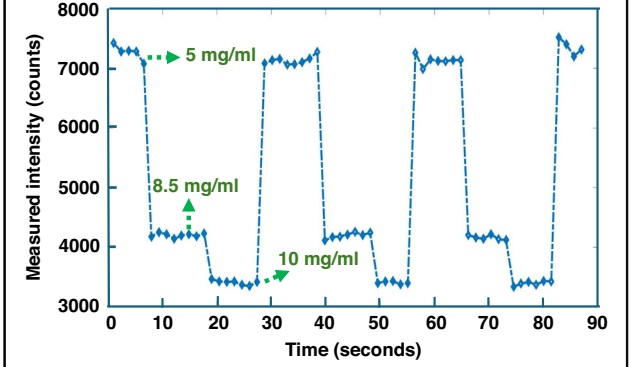


**Fig. 14** Transient response of $HPTS_{88}Ru$ during change in oxygen concentrations from 5.0 to 10.0 mg/ml

zero sensitivity at 520 nm. The oxygen sensitivity is calculated to be approximately 20.4% per mg/ml. The insensitive 520 nm peak is of high significance in this study. This result ensures that a single sensor can deliver two independent signal outputs, one for pH and the other for oxygen, respectively, without any evident interference.

Considering a normoxic tissue, the ratio of intensity of the 600 nm emission peak (due to oxygen) to the intensity of the 520 nm emission peak (due to pH) was found to be 0.71. In this case, the pH was 7.6 and oxygen concentration 8.5 mg/ml. In case of hypoxic tissue (pH = 6.6 and oxygen concentration = 5 mg/ml), the ratio increased to approximately 2, i.e. almost 2.8 times higher than for the normoxic tissue. Thereby, by analysing the peak intensity ratio, we can determine the oxygen status of the tissue or organ.

Figure 13 shows the transient real-time response of the $HPTS_{88}Ru$ sensor towards change in pH levels of the solution from 7.0 to 7.6. The sensor was initially exposed to a solution of pH value 7.0 for ten minutes. The sensor was then withdrawn from the 7.0 pH solution and exposed to a solution of pH 7.6. When the sensor is illuminated with 405 nm light, the phenolic groups in the HPTS absorb more light at higher pH. This results in higher fluorescence intensity, as shown in Fig. 10. The sensor exhibits a very-short pH response time of 12.5 s, making it appropriate for medical applications.

Figure 14 shows the transient real-time response of the $HPTS_{88}Ru$ sensor towards change in oxygen concentration of the solution from 5 mg/ml to 10 mg/ml. The higher the concentration of oxygen in solution, the higher

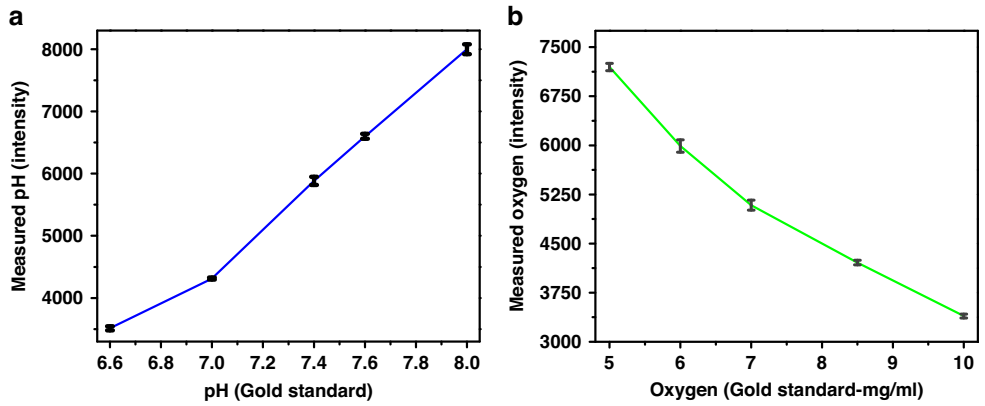


**Fig. 15 Calibration curve of $HPTS_{88}Ru$. a** For pH (b) for oxygen

the number of collisions between the excited states of ruthenium and oxygen molecules.

The concentration-dependent collision rate is responsible for the fluorescence quenching at 600 nm during oxygen sensing. The sensor exhibits oxygen response time of less than 2 s, which makes it ideal for detecting quick alterations. The fabricated bi-functional sensor demonstrated an intensity ratio of 2.0 in hypoxic conditions and 0.71 in normoxic conditions, signifying its applicability in identifying damaged tissues. Finally, the stability of the sensor was confirmed during three subsequent cycles of measurement.

Figures 15a and b represents the calibration curve of $HPTS_{88}Ru$ sensor towards pH and oxygen, respectively. As discussed earlier, the intensity for pH is observed to increase with increased pH values, whereas the oxygen intensity reduces with increase in oxygen concentration. The pH and oxygen levels were measured and standardized using a pH meter and dissolved oxygen meter, respectively.

### Preliminary measurements on human tissue and future scope

Figure 16 shows the unviable human liver, declined for transplantation in the Erasmus Medical Centre, Rotterdam, the Netherlands.

Figure 17 shows the results of oxygen and pH measurements on human tissue. The sensor exhibited a decrease in fluorescence intensity with manually increased oxygen concentration in the perfusate (Fig. 17a). When discontinuing the oxygen supply, a decrease in pH intensity can be observed (Fig. 17b).

Finally, the drift analysis of the sensor was performed to evaluate the sensor stability. Figure 18a demonstrates the sensor stability when subjected to a solution of pH 7.0 for 8 minutes. The sensor showed good stability for 5.5 minutes which is sufficient for detecting tissue vitality.

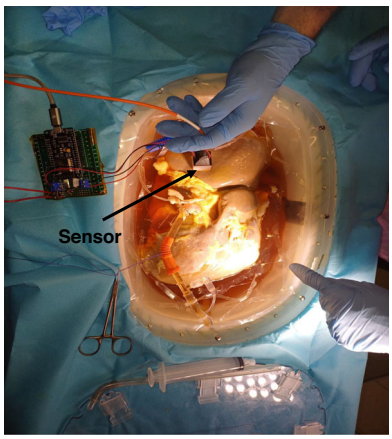


**Fig. 16** Initial test carried out to detect oxygen and pH levels in human liver declined for transplantation

Figure 18b demonstrates the intensity ratio of the sensor when exposed to i) pH=6.6 and oxygen= 5 mg/ml (mimicking damaged tissue condition) and ii) pH=7.4 and oxygen = 10 mg/ml (mimicking healthy conditions). The intensity ratio of oxygen and pH eliminates the drift of the sensor towards pH and oxygen with time. Therefore, long-lasting, continuous monitoring, intensity measurements are highly preferred to individual, segmented monitoring of parameters.

These preliminary measurements provided the initial successful demonstration of functionality and application of the sensor. Further miniaturization of this sensor along with additional characterization is essential for successful implementation during organ perfusion. The integration of a pH and oxygen sensor into a perfusion set up could enhance our understanding of microcirculation by capturing regional differences and bridging the gap between systemic delivery and local tissue perfusion.

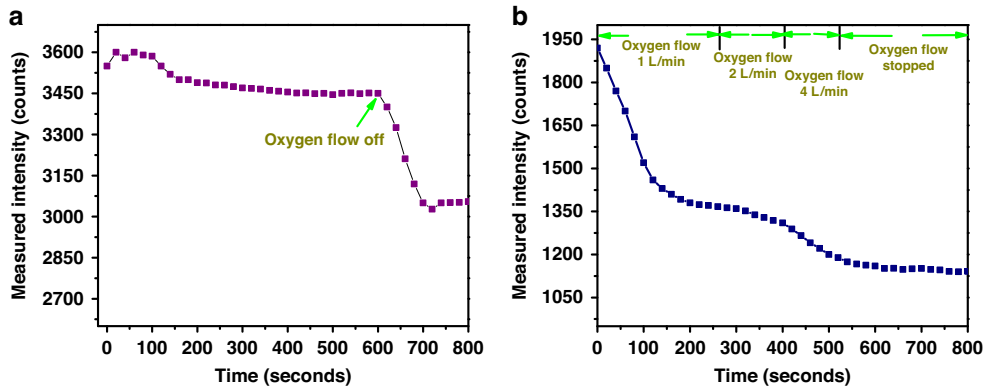


**Fig. 17 Initial test carried out in human liver. a** Changes in pH intensity with change in oxygen supply (**b**) changes in oxygen intensity with oxygen flow rate

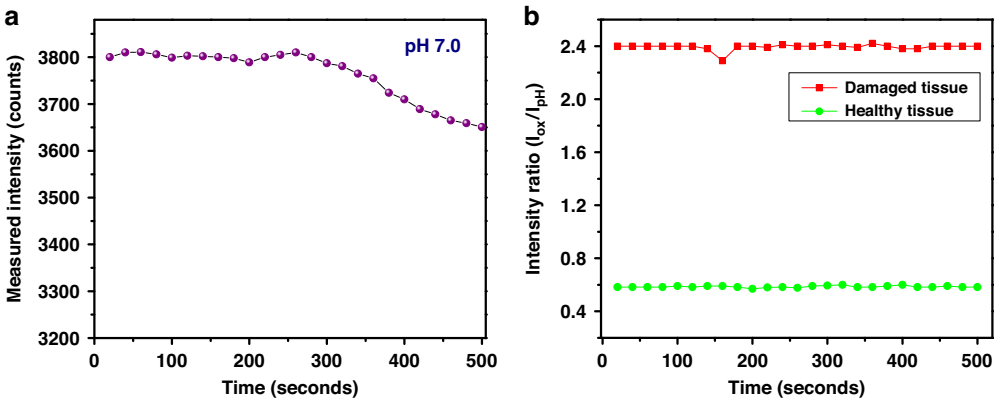


**Fig. 18 Sensor stability. a** Stability of the HPTS88Ru sensor (**b**) stability of the sensor during measurement of intensity ratio

## Conclusions

We presented a novel optical sensor which can detect changes in the pH and oxygen levels at the same time. The sensor was optimized meticulously to avoid any cross-sensitivity during pH and oxygen measurements. The sensor exploits a single excitation at 405 nm, and is characterized by dual emission at 520 nm and 600 nm, respectively corresponding to pH and oxygen variations. The fast response of the sensor towards pH and oxygen is attributed with a response time of 12.5 s and 1.4 s respectively. The sensor exhibits a sensitivity of 75.75% for pH variations and 20.4% per mg/ml for changes in oxygen concentration. Further development of this sensor may enhance the ability to monitor microcirculatory perfusion within organs.

#### Acknowledgements

The authors would like to extend their heartfelt gratitude towards "Flagship Convergence Project" (a collaboration between TU Delft, Erasmus Medical Centre and Erasmus University) for funding this research. The authors would like to thank Brian Nanhekhan for his extended support during measurements. The authors would also like to acknowledge the contribution of EKL support staff at TU Delft, for experimental support.

#### Author details

[1]Department of Microelectronics, Delft University of Technology, Mekelweg 4, 2628 CD Delft, The Netherlands. [2]School of Electrical and Computer Sciences, Indian Institute of Technology (IIT), Bhubaneswar, India. [3]Erasmus MC Transplant Institute, University Medical Center Rotterdam, Department of Surgery, Division of HPB and Transplant Surgery, Rotterdam, The Netherlands

#### Author contributions

A.S. designed the research, developed the sensor, performed the measurements and wrote the manuscript. F.B assisted in measurements and sensor design, P.G and A.M. provided medical insights, valuable corrections to the manuscript, and arranged the liver experiment, J.J assisted in medical information and arranged for the liver experiment, R.F. assisted in the material synthesis and measurement. M.M. provided guidance in measurements, discussed sensor characteristics, and contributed in manuscript preparation. P.F provided overall guidance and helped in developing the research. All authors discussed the results and have given approval to the final version of the manuscript.

#### Conflict of interest

The authors declare no competing interests.

## Ethics

All experiments on human organs have been approved by 'The local medical ethics committee of the Erasmus MC approved the use human organs (MEC-2012-090).' This is in compliance with Dutch law.

Received: 27 October 2025 Revised: 5 May 2026 Accepted: 22 May 2026
Published online: 28 August 2026

## References

1. Groen, P. C., Van Leeuwen, O. B., De Jonge, J. & Porte, R. J. Viability assessment of the liver during ex-situ machine perfusion prior to transplantation. *Curr. Opin. Organ Transplant.* **29**, 239–247 (2024).
2. Watanabe, T. atsuaki, Cypel, M. arcelo & Keshavjee, S. haf Ex vivo lung perfusion. *J. Thorac. Dis.* **13**, 6602 (2021).
3. Clark, L. C. & Lyons, C. Electrode systems for continuous monitoring in cardiovascular surgery. *Ann. NY Acad. Sci.* **102**, 29–45 (1962).
4. J. R. Lakowicz, "Chapter 9: Advanced topics in fluorescence quenching," in *Principles of Fluorescence Spectroscopy*, 2nd ed. New York: Plenum, 1999, pp. 267–289.
5. Choi, M. M. F. & Xiao, D. Single standard calibration for an optical oxygen sensor based on luminescence quenching of a ruthenium complex. *Anal. Chim. Acta* **403**, 57–65 (2000).
6. O. S. Wolfbeis, M. J. P. Leiner, and H. E. Posch, "A new sensing material for optical oxygen measurement, with the indicator embedded in an aqueous phase," *Mikrochim. Acta*, III, 359–366, 1986.
7. Klimant, I. & Wolfbeis, O. Oxygen-sensitive luminescent materials based on silicone-soluble ruthenium diimine complexes. *Anal. Chem.* **67**, 3160–3166 (1995).
8. Li, X.-M., Ruan, F.-C. & Wong, K.-Y. Optical characteristics of a ruthenium(II) complex immobilized in a silicone rubber film for oxygen measurement. *Analyst* **118**, 289–292 (1993).
9. Gouin, J. F., Baros, F., Birot, D. & André, J. C. A fiber-optic oxygen sensor for oceanography. *Sens. Actuators B* **38–39**, 401–406 (1997).
10. Miyashita, T., Chen, J., Yuasa, M. & Mitsuishi, M. Fabrication of polymer organized thin films containing ruthenium complexes. *Polym. J.* **31**, 1121–1126 (1999).
11. Preininger, C., Klimant, I. & Wolfbeis, O. S. Optical fiber sensor for biological oxygen demand. *Anal. Chem.* **66**, 1841–1846 (1994).
12. McNamara, K. P., Li, X., Stull, A. D. & Rosenzweig, Z. Fiber-optic oxygen sensor based on the fluorescence quenching of tris (5-acrylamido, 1,10 phenanthroline) ruthenium chloride. *Anal. Chim. Acta* **361**, 73–83 (1998).
13. Singer, E., Duveneck, G. L., Ehrat, M. & Widmer, H. M. Fiber optic sensor for oxygen determination in liquids. *Sens. Actuators A* **41–42**, 542–546 (1994).
14. W. Wang, C. E. Reimers, S. C. Wainwright, M. Shahriari, and M. J. Morris, "Applying fiber-optic sensors for monitoring dissolved oxygen," *Sea Technol.*, pp. 69–74, 1999.
15. Malins, C., Niggeman, M. & MacCraith, B. D. "Multi-analyte optical chemical sensor employing a plastic substrate. *Meas. Sci. Technol.* **11**, 1105–1110 (2000).
16. Ingersoll, C. M. & Bright, F. V. "Using sol-gel-based platforms for chemical sensors. *Chemtech* **21**, 26–31 (1997).
17. MacCraith, B. D., O'Keeffe, G., McDonagh, C. & McEvoy, A. K. LED-based fiber optic oxygen sensor using sol-gel coating. *Electron. Lett.* **30**, 888–889 (1994).
18. Krihak, M. K. & Shahriari, M. R. Highly sensitive, all solid state fiber optic oxygen sensor based on the sol-gel coating technique. *Electron. Lett.* **32**, 240–241 (1996).
19. Shahriari, M. R., Ding, J. Y., Tong, J. & Sigel, G. H. Jr Sol-gel coating based fiber optic O /DO sensors. *Proc. SPIE* **2068**, 224–240 (1994).
20. Baker, G. A., Wenner, B. R., Watkins, A. N. & Bright, F. V. Effects of processing temperature on the oxygen quenching behaviour of tris(4, 7 -diphenyl-1, 10 -phenanthroline) ruthenium (II) sequestered within sol-gel-derived xerogel films. *J. Sol.-Gel Sci. Technol.* **17**, 71–82 (2000).
21. Wolfbeis, O. ttoS. An overview of nanoparticles commonly used in fluorescent bioimaging. *Chem. Soc. Rev.* **44**, 4743–4768 (2015).
22. McEvoy, A. K., McDonagh, C. M. & MacCraith, B. D. Dissolved oxygen sensor based on fluorescence quenching of oxygen-sensitive ruthenium complexes immobilized in sol–gel-derived porous silica coatings. *Analyst* **121**, 785–788 (1996).
23. Lin, H. et al. Strain and humidity insensitive, stretchable hydrogel-based oxygen sensor with corrosion-free electrodes for wireless oxygen detection. *Sens. Actuator B: Chem.* **414**, 135939 (2024).
24. Kermis, H. R., Kostov, Y. & Rao, G. Rapid method for the preparation of a robust optical pH sensor. *Analyst* **128**, 1181–1186 (2003).
25. De Graaf, G. er, Vriesendorp, M. F., Hassan, H. M. A. & French, P. J. Opto-Chemical pH Detection of Myocardial Ischaemia Using Fluorescent Hydrogels. *IEEE Sens. J.* **22**, 10901–10909 (2022).
26. Kalogeris, T., Baines, C. P., Krenz, M. & Korthuis, R. J. Ischemia/reperfusion. *Compr. Physiol.* **7**, 113–170 (2017).
27. Kalogeris, T., Baines, C. P., Krenz, M. & Korthuis, R. J. Cell biology of ischemia/reperfusion injury. *Int. Rev. cell Mol. Biol.* **298**, 229–317 (2012).
28. Boedtkjer, E. & Ara, T. Strengthening the basics: acids and bases influence vascular structure and function, tissue perfusion, blood pressure, and human cardiovascular disease. *Pflügers Arch.-Eur. J. Physiol.* **476**, 623–637 (2024).
29. Schuiringa, G. H., Mihajlovic, M., Van Donkelaar, C. C., Vermonden, T. & Ito, K. Creating a functional biomimetic cartilage implant using hydrogels based on methacrylated chondroitin sulfate and hyaluronic acid. *Gels* **8**, 457 (2022).
30. Ge, X., Kostov, Y. & Rao, G. High-stability non-invasive autoclavable naked optical CO2 sensor. *Biosens. Bioelectron.* **18**, 857–865 (2003).
31. Haller, H. L. et al. Oxygen, pH, Lactate, and Metabolism-How Old Knowledge and New Insights Might Be Combined for New Wound Treatment. *Med. (Kaunas.)* **57**, 1190, https://doi.org/10.3390/medicina57111190 (2021).
32. She, D. & Allen, M. G. A self-powered, biodegradable dissolved oxygen microsensor. *J. Microelectromechanical Syst.* **29**, 1074–1078 (2020).
33. Chan, C. M., Lo, W. & Wong, K. Y. Application of a luminescence-based pH optrode to monitoring of fermentation by Klebsiella pneumoniae. *Biosens. Bioelectron.* **15**, 7–11 (2000).
34. Kerry, P. M., Li, X., Angela, D. S. & Zeev, R. Fiber-optic oxygen sensor based on the fluorescence quenching of tris (5-acrylamido, 1, 10 phenanthroline) ruthenium chloride. *Analytica Chim. acta* **361**, 73–83 (1998).
35. Buehler, S. M. et al. Cell monitoring and manipulation systems (CMMSs) based on glass cell-culture chips (GC3s). *Micromachines* **7**, 106 (2016).
36. Gray, M. E. et al. In vivo validation of a miniaturized electrochemical oxygen sensor for measuring intestinal oxygen tension. *Am. J. Physiol.-Gastrointest. Liver Physiol.* **317**, G242–G252 (2019).
37. Francone, A. et al. Integrated 3D hydrogel waveguide out-coupler by step-and-repeat thermal nanoimprint lithography: A promising sensor device for water and pH. *Sensors* **18**, 3240 (2018).
38. O'Neal, D. et al. Oxygen sensor based on the fluorescence quenching of a ruthenium complex immobilized in a biocompatible poly (ethylene glycol) hydrogel. *IEEE Sens. J.* **4**, 728–734 (2004).
39. Mayevsky, A. vraham et al. Tissue spectroscope: a novel in vivo approach to real time monitoring of tissue vitality. *J. Biomed. Opt.* **9**, 1028–1045 (2004).